SLAC–PUB–17261

High-power Femtosecond soft X-rays from Fresh-slice Multi-stage Free-Electron Lasers

Alberto A. Lutman†, Marc W. Guetg, Timothy J. Maxwell, James P. MacArthur,
Marc W. Guetg, Yuantao Ding, Claudio Emma,
Jacek Krzywinski, Agostino Marinelli and Zhirong Huang
SLAC National Accelerator Laboratory, Menlo Park, CA 94025

Abstract

We demonstrate a novel multi-stage amplification scheme for self-amplified spontaneous-emission Free Electron Lasers for the production of few femtosecond pulses with very high power in the soft X-ray regime. The scheme uses the fresh-slice technique to produce an X-ray pulse on the bunch tail, subsequently amplified in downstream undulator sections by fresh electrons. With three-stages amplification, X-ray pulses with an energy of hundreds of microjoules are produced in few femtoseconds. For single-spike spectra X-ray pulses the pulse power is increased more than an order of magnitude compared to other techniques in the same wavelength range.

Physical Review Letters, accepted for publication 14th May 2018.
Work supported by the U.S. Department of Energy, Office of Science, Laboratory Directed Research and Development (LDRD) program at SLAC National Accelerator Laboratory, under contract DE-AC02-76SF00515.

† aal@slac.stanford.edu

X-ray Free Electron Lasers (XFEL) are the brightest sources of X-rays for scientific applications[1–5]. XFELs are used in several fields of scientific investigation, including biology, chemistry, matter in extreme conditions, condensed matter physics and atomic, molecular, and optical physics[6, 7]. Existing FEL machines capable of operating in the X-rays are based either on Self-Amplified Spontaneous Emission (SASE)[8, 9] or in the High Gain Harmonic Generation (HGHG) scheme[10]. HGHG machines present better temporal coherence and wavelength stability, but have so far only produced softer X-rays down to 4 nm wavelength[11]. SASE machines can produce harder X-rays, operating at fundamental wavelengths down to 1 Å.

The XFEL pulse shaping is an active field of investigation to enable experiments requiring X-rays with tailored temporal profiles, spectra and polarization. X-ray pump, X-ray probe experiments (see e.g. Refs [12, 13]) were enabled by double-pulse schemes[14–20]; narrow-band and wavelength stability were improved for SASE machines with the Self-Seeding schemes[21–24]. Polarization control was achieved with variable polarization undulators like the Apple-II[3, 25] and the Delta[26], and coherent phase control between different HGHG harmonics was demonstrated at FERMI[27].

Recently, the highest achievable power at an FEL has been improved in the hard X-rays by correcting the electron bunch tilt[28] with a collimated beam[29], and production of sub-femtosecond pulses was demonstrated[30, 31] in the same wavelength range. High power ultra-short pulses are required for single-particle imaging [32, 33], femtosecond X-ray cristallography and X-ray spectrocopy [34, 35] to exploit the probe before destroy principle.

In the soft X-rays wavelengths, XFELs have also revealed a variety of nonlinear phenomena when intense X-ray pulses interact with atoms and molecules [36, 37]. These include stimulated X-ray emission [38, 39], where an increase of a few times in peak intensity can lead to a signal increase of several orders of magnitude. Producing intense pulses with durations lower than the Auger decay lifetimes (~ 5 fs) would enable the generation of double core-hole states[40] in low Z materials to investigate the fine electronic structures in the fields of chemistry and biology.

At soft X-rays wavelengths, the slotted foil technique[41] can produce few-femtosecond pulses[42, 43] with an energy of few tens of microjoule. However to produce a reliable rate of single coherent spectral spikes, the operating point should be kept before saturation thereby limiting the achievable power. Several schemes have been proposed to produce high power

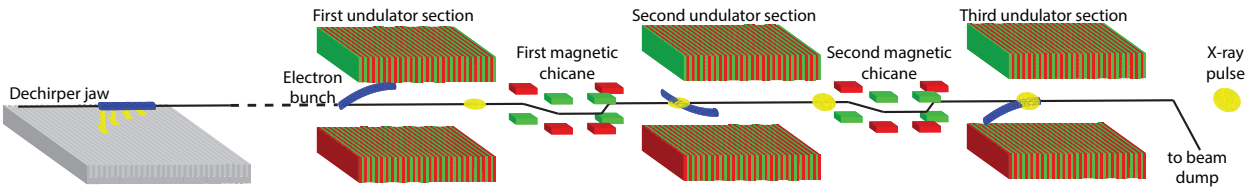

FIG. 1. The electron bunch travelling close to a metal corrugated jaw of the dechirper experiences a strong transverse head-tail kick (yellow arrows). The bunch orbit is controlled to have a tail slice travelling straight in the first undulator section. A magnetic chicane delays the electron bunch to overlap the photon pulse in the first section with fresh-electrons toward the bunch core. In the second undulator section the X-ray pulse is amplified by fresh-electrons. A second magnetic chicane delays the electron bunch to overlap the photon pulse with fresh-electrons on the bunch head. In the third undulator section the X-ray pulse is amplified by fresh-electrons on the bunch head.

ultra-short soft X-rays [44–50]. Particularly, a multi-stage scheme capable of generating terawatt few-femtosecond pulses has been proposed[47] by using Fresh-slice amplification in ten cascaded stages.

The Fresh-slice technique[18] consists in controlling which temporal slice of an electron bunch lases in each undulator section without spoiling the other slices as with the emittance spoiler[41] or optical laser heater shaping[51]. Such control has been achieved with an electron bunch tailored with a temporal-transverse correlation impressed by the transverse wakefields of a dechirper[52]. Alternatively a radio-frequency deflector and a dispersion based method could also induce the required time-dependent orbit[53]. Recently, a transverse matching-based scheme[54] has also been studied in simulations[55] to avoid large electron bunch orbits in the undulator line.

In this Letter we demonstrate a multi-stage SASE amplification scheme[47] producing high-power few femotosecond pulses using two or three amplification stages. With two stages, about 25% of the shots present a single spectral spike with a pulse energy close to a hundred microjoules, a few times larger compared to single-spikes produced so far with other methods in the same wavelength range. With three stages, pulses with an energy of hundreds of microjoules are produced in a few femtoseconds. The single spectral spike shots have a rate of 13% with a power more than an order of magnitude larger over competing methods in the same wavelength range. The remaining 87% X-ray pulses are still characterized by

high power and short temporal durations of few femtoseconds, but present mostly two or three spectral spikes.

In an XFEL, X-rays are produced by a high-current, low emittance electron bunch travelling in an undulator. The radiation wavelength λ_r depends on the undulator period λ_u, the undulator strength parameter K, and the Lorentz factor of the electron bunch γ as $\lambda_r = \lambda_u \frac{1+K^2/2}{2\gamma^2}$. At the LCLS[1] the typical electron bunch has a charge of 180 pC at the exit of the linear accelerator, and has a peak current ranging from 500 A to 5 kA. The electron bunch energy range, from 2.5 GeV to 17 GeV, allows production of X-rays with photon energies between 280 eV and 12.9 keV.

A dechirper system[56, 57] was installed 120 m upstream of the entrance of the undulator line to control the electron bunch time-energy longitudinal distribution. Longitudinal phase space control with a dedicated wakefield device had been also previously demonstrated at other facilities [58–62]. The system is composed by two 2-m long modules, one vertical and one horizontal. Each module has a pair of corrugated aluminum plates, suitable to produce strong short range wakefields.

A single corrugated metal jaw close to the electron bunch is sufficient to impress the required head-tail kick. Nevertheless, it is still useful to use both modules to mitigate the time-correlated quadrupole defocusing[61] and to have a better FEL suppression by tilting the electron bunch in both horizontal and vertical directions.

Figure 1 is a schematic of the multistage amplification experiment. The electron bunch travels close to a corrugated aluminum jaw of the dechirper and receives a nonlinear time-correlated head-tail transverse kick. The bunch slices on the head are subject to negligible transverse wakefield. The slices at the bunch tail are subject to a strong transverse kick toward the metal jaw. In the downstream strong focusing lattice, the slices toward the bunch tail perform betatron oscillations. The amplitude of the oscillations depends on the longitudinal position within the bunch, with smaller oscillations toward the bunch head. Prior to entering the undulator line, the electron bunch orbit is steered such that a temporal slice on the bunch tail travels straight, while core and head slices travel on increasing oscillating orbits. A short X-ray pulse is produced by the electrons on the tail. The first chicane delays the electron bunch by few femtoseconds to overlap the X-ray pulse with fresh-electrons toward the bunch core. The electron bunch orbit is adjusted to have the corresponding slice on the bunch core travelling straight in the second undulator section. The high-power ultra-

short seed impresses a strong modulation to the fresh-electrons and a strong post-saturation taper is applied in the second section. Besides being optimized for the growth of the seeded pulse, the second stage taper also further suppresses the FEL growth for electrons that travel on very small oscillating orbits, but are not overlapped with the short seed produced in the upstream stage. The second magnetic chicane delays the electron bunch to overlap the X-ray pulse on fresh-electrons on the bunch head, the electron bunch orbit is adjusted accordingly, and strong post-saturation taper is also applied in the third undulator section. The existing LCLS layout limits the number of possible stages to three.

The experimental demonstration for two-stage amplification was performed operating at 670 eV, with electron bunches at an energy of 3900 ± 3.2 MeV, a peak current of 4100 ± 380 A. The electron bunch charge after collimation[29] in the first bunch compressor was 142.4 ± 2.4 pC. The electron bunch was tuned to lase uniformly, producing SASE pulses of a duration of ~ 35 fs and an energy of 650 μJ in the first 8 undulator segments. In such condition the electron bunch was travelling on the zero Beam Position Monitor (BPM) orbit corresponding to the undulator line axis. Both horizontal and vertical dechirpers were used to tailor the electron bunch with the temporal-transverse correlation. The horizontal and vertical jaws of the dechirper were set as close to the electron bunch as possible to operate the machine without electron bunch charge losses. The other two jaws were left fully retracted, thus having a negligible interaction with the electron bunch. In the described condition, the electron bunch was lasing only on the bunch head and the head lasing orbit was recorded.

The first stage was tuned to lase on the far tail of the electron bunch and produced on average 9 μJ pulses, in the first 8 undulators. The pulse power on the tail is lower compared to the one of the full-lasing bunch because of the transverse time-dependent mismatch. However, it is several orders of magnitude larger than electrons shot noise and sufficient to start the lasing process in the second stage close to saturation. The magnetic chicane was then used to overlap the photon pulse with fresh-electrons, and the orbit was empirically steered to set the corresponding electron bunch slice on the straight orbit. The second section was 6 undulator segments long, and a strong quadratic taper was applied on the entire section. Figure 2 shows the experimental results for the second stage using two different delay settings: 7 fs and 3 fs. On 100 consecutive shots the pulse intensity was measured as 165 ± 59 μJ and 77 ± 33 μJ, for the 7 and 3 fs delay cases respectively. With the shorter delay, only the head of the pulse produced in the first stage actually overlaps

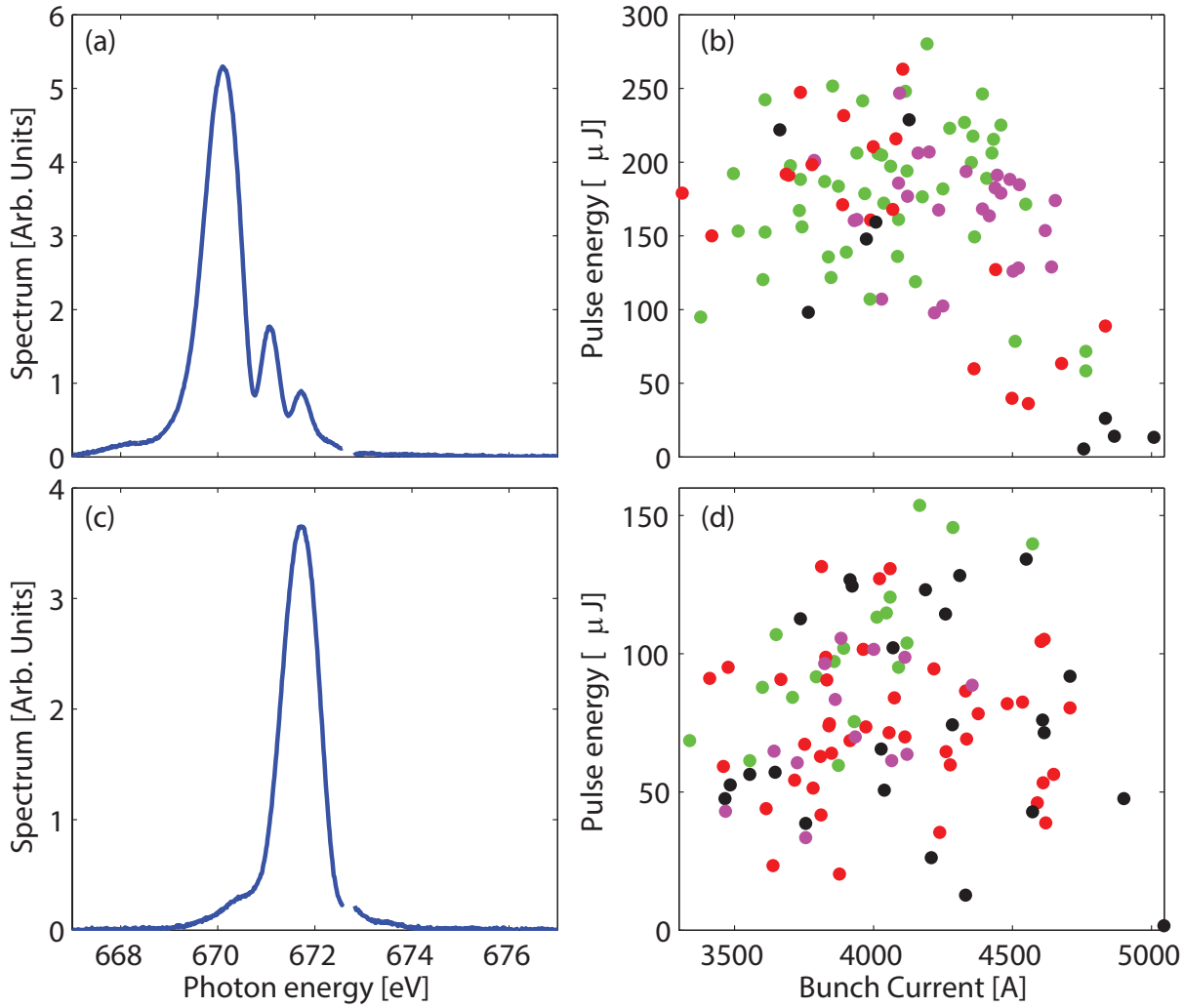

FIG. 2. Two-stage amplification experimental data, with 7 fs chicane delay (a,b) and with 3 fs chicane delay (c,d). Examples of single-shot measured spectra (a,c). Few energies close to 673 eV were removed from the plot because of a crack on the spectrometer detector. X-ray pulse energy vs electron bunch current (b,d). Color coding is used for spectra having a different number of spikes. 1 spike (black), 2 spikes (red), 3 spikes (green), more than three spikes (magenta)

fresh-electrons in the second stage, therefore allowing shorter albeit weaker pulses. Figure 2(a,c) show single-shot spectra measured with a grating spectrometer[63, 64]. The 7 fs delay sample had three spikes and an energy of 211μJ, while the 3 fs delay sample had 125 μJ with a single-spike spectrum. The pulse structure was analyzed for a set of 100 consecutive shots in each condition. Each X-ray pulse spectrum was fitted with multiple Gaussians, and the number of spikes was calculated as the one for which the cumulative spectral energy

was above 90%. Table I reports the number of spike rates for the different sets. In the 3 fs case, roughly one pulse out of four presents a single spike, such rate increases to 37% if the cumulative energy threshold is set to 85%. Figures 2(b,d) show the distribution of the pulse energies with respect to the electron bunch peak current. Spectra with different number of spikes are coded with different colors, and intense X-ray pulses with few spectral spikes can be found in both analyzed sets.

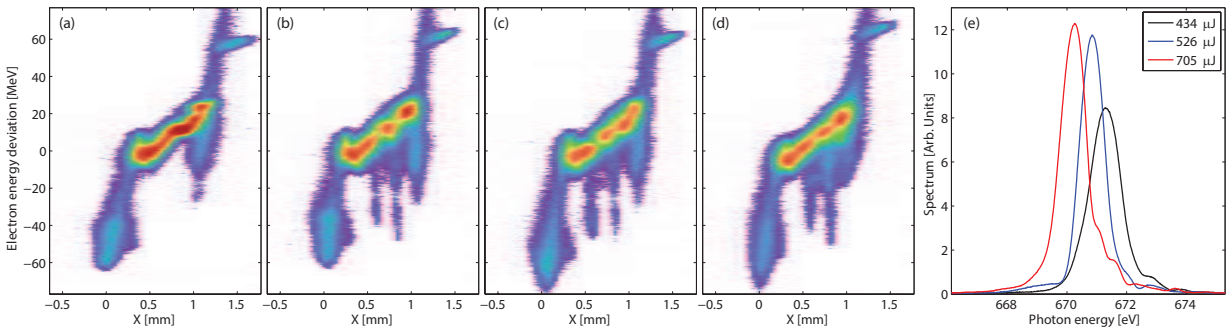

FIG. 3. Example of single-shot electron bunch phase space with lasing suppressed (a). Examples of single-shot electron bunch phase spaces for three-stage amplified SASE pulses (b-d), bunch energy is relative to 4 GeV. The X coordinate on the screen represents time. The temporal scale is non-linear due to the horizontal dechirper wake effect and has been left in mm at the screen. The full bunch length is approximately 35 fs. The footprints of the second and third stage amplification are visible in the core of the bunch, the first stage had too low power to produce a clear footprint. Bunch head is on the right. Corresponding single-shot spectra (e). Black, blue and red corresponds to b,c and d, respectively.

A similar machine setup was used to perform a three stage amplification experiment at an energy close to 670 eV. The electron bunch energy was 3882 ± 2.6 MeV, the peak current was 3780 ± 370 A and the charge at the end of the linac was 135 ± 1.9 pC. 8, 6 and 9 undulator segments were used in the first, second and third section, respectively. The first and second magnetic chicane delays were both set to 4 fs, and the orbit of the electron bunch in the second and third sections were adjusted in accord with the chicane delays. Quadratic post-saturation taper was applied from the fifth segment in the first section. The undulator strength of the first segment in each downstream section was empirically set to be on resonance, considering that the electron bunch presented a chirped energy profile. Finally, a strong post-saturation taper was applied from the second segment in the other

sections, empirically optimizing the observed signal on the spectrometer's detector.

Figure 3 shows the experimental results for three single-shots recorded with this setup. Figures 3(a) shows a measured lasing-off electron bunch phase space. 3(b-d) show the measured time-resolved electron bunch phase spaces downstream of the lasing process. In the figures the horizontal coordinate is correlated with the time along the electron bunch by the transverse deflection from the X-band Transverse Cavity (XTCAV)[42] and the horizontal transverse wakefields. However, since a strong nonlinear deflection was imparted by the horizontal wakefield of the dechirper, an accurate determination of the time-axis would require a careful analysis with the tools developed for passive streaking as electron bunch diagnostic[65, 66]. Therefore the horizontal axis was left in units of millimeters at the screen. In each phase space, the first stage amplification is barely visible on the bunch tail (on the left). The second and the third stage lasing footprints are instead very well defined in the core of the electron bunch. The remaining two features at the far-tail and the head of the bunch are wide-energy spread charge distribution horns that do not contribute significantly to the lasing process. Figure 3(e) shows the measured single-shot single-spike spectra for the three presented phase spaces. With an energy of several hundreds of microjoules, the single-spike spectra have an energy of more than an order of magnitude larger compared to the ones generated by other techniques, such as low charge and slotted foil, in the same range of wavelengths. The FWHM bandwidths for the three presented shots are of 1.19 eV, 0.95 eV and 1.00 eV, with respective pulse energy of 434, 526 and 705 μJ. For a Fourier transform limited Gaussian pulse, a bandwidth of 1 eV FWHM corresponds to a duration

TABLE I. Analysis of spectral structure for the two-stage amplification scheme on 100 consecutive X-ray pulses. The Rate 3 fs and Rate 7 fs refers to pulses recorded with a chicane delay of 3 and 7 fs, respectively. Others may refer to shots with more than three spikes, too low intensity to be analyzed, or partially outside of the spectrometer range.

Number of spikes	Rate, 3 fs delay	Rate, 7 fs delay
1	24%	9%
2	42%	19%
3	19%	46%
others	15%	26%

of ~ 1.8 fs FWHM. In the case of multi-stage amplified pulses further studies are required to assess the shape and the frequency chirp of the pulses. However, single spectral spikes and the resolved electron bunch phase spaces point to pulse durations of few femtoseconds, since the duration between lasing footprints of the second and third stage is close to the four femtoseconds set by the magnetic chicane delay. The rate of single-spikes spectra in the three stage configuration is lower compared to the two-stage one. On 500 consecutive shots, 63 (12.6%) X-ray pulses were single-spikes and 178 presented a double spike structure, as summarized in Table II. About half of the single-spike shots had a large pulse energy above 300 μJ.

The X-ray pulse duration of the multi-stage amplified pulses can be controlled by the selection of the position of the lasing slice within the bunch and by the undulator taper. Shorter pulses are produced by starting on a slice on the farther tail, shorter delay stages and steeper quadratic taper. A shallower taper allows weaker spikes to catch up with stronger ones, eventually up to the point where the entire temporal slice lases, even if starting from shot noise. A steeper taper instead, amplifies well only the stronger XFEL spikes from the previous stage. For example, a longer pulse duration three stage configuration was developed at the same photon energy with an average X-ray pulse energy of 619 μJ on 100 consecutive shots. The phase space of an intense shot of 1.1 mJ was analyzed resulting in a ~ 5.7 fs FWHM long third stage lasing footprint, neglecting the horizontal wakes effect.

The XTCAV based temporal X-ray reconstruction for such pulses may be inaccurate for several reasons, including the fact that losses from different bunch slices cooperate to build a single short pulse, slippage effects, non-linearity of the time axis when the horizontal dechirper is in use, and resolution limit. A reliable measurement of the produced X-ray

TABLE II. Analysis of spectral spikes structure for the three-stage amplification scheme on 500 consecutive X-ray pulses.

Number of spikes	Rate	Pulse energy
1	13%	304 ± 117 μJ
2	36%	299 ± 113 μJ
3	36%	289 ± 115 μJ
others	15%	235 ± 123 μJ

pulses could be performed with the angular streaking method that recently achieved sub-femtosecond resolution[67, 68]. Such measurement could also provide single-shot information to sort-out the stochastic properties of the spectral structure for an experiment. There is also the possibility of applying machine learning algorithms to predict additional information on the spike structure, on single shot basis, by analyzing the XTCAV and machine data[69].

In summary, we demonstrated a novel multi-stage amplification scheme capable of producing few femtosecond X-ray pulses, featuring high-power and a reliable rate of single-spike spectra. With the current machine layout, three stage operation is limited to photon energies up to 1.6 keV. The length of the undulator sections with present chicane locations may be too short to operate at higher photon energies due to gain-length increase. Performance could be further improved with a different machine layout, allowing a larger number of amplification stages, with shorter chicanes, or by combining it with schemes capable of generating electron bunches with a train of high-current spikes[44, 70]. Further work will be required to better extract quantitative information on the X-rays from the time-resolved electron bunch measurements downstream of the undulator line.

We thank Prof. C. Bostedt for the useful discussions. This work was supported by the U.S. Department of Energy, Office of Science, Laboratory Directed Research and Development (LDRD) program at SLAC National Accelerator Laboratory, under contract DE-AC02-76SF00515.

[1] P. Emma *et al.*, Nat. Photon. **4**, 641 (2009).

[2] T. Ishikawa *et al.*, Nat. Photon. **6**, 540 (2012).

[3] E. Allaria *et al.*, Nat. Photon. **6**, 699 (2012).

[4] W. Ackermann *et al.*, Nat. Photon. **1**, 336 (2007).

[5] H.-S. Kang *et al.*, Nat. Photon. **11**, 708 (2017).

[6] C. Bostedt, S. Boutet, D. M. Fritz, Z. Huang, H. J. Lee, H. T. Lemke, A. Robert, W. F. Schlotter, J. J. Turner, and G. J. Williams, Rev. Mod. Phys. **88**, 015007 (2016).

[7] U. Bergmann, V. Yachandra, and J. Yano, eds., *X-Ray Free Electron Lasers*, Energy and Environment Series (The Royal Society of Chemistry, 2017) pp. P001–463.

[8] Y. Derbenev, A. Kondratenko, and E. Saldin, Nuclear Instruments and Methods in Physics

Research **193**, 415 (1982).

[9] R. Bonifacio, C. Pellegrini, and L. M. Narducci, Optics Communications **50**, 373 (1984).

[10] L. H. Yu, Phys. Rev. A **44**, 5178 (1991).

[11] E. Allaria *et al.*, Nat. Photon. **7**, 913 (2013).

[12] K. R. Ferguson *et al.*, Science Advances **2** (2016), 10.1126/sciadv.1500837.

[13] A. Picón *et al.*, Nature Communications **7**, 11652 EP (2016), article.

[14] A. A. Lutman, R. Coffee, Y. Ding, Z. Huang, J. Krzywinski, T. Maxwell, M. Messerschmidt, and H.-D. Nuhn, Phys. Rev. Lett. **110**, 134801 (2013).

[15] T. Hara *et al.*, Nature Communications **4**, 2919 (2013).

[16] A. Marinelli, A. A. Lutman, J. Wu, Y. Ding, J. Krzywinski, H.-D. Nuhn, Y. Feng, R. N. Coffee, and C. Pellegrini, Phys. Rev. Lett. **111**, 134801 (2013).

[17] A. Marinelli *et al.*, Nature Communications **6**, 6369 (2015).

[18] A. A. Lutman, T. J. Maxwell, J. P. MacArthur, M. W. Guetg, N. Berrah, R. N. Coffee, Y. Ding, Z. Huang, A. Marinelli, S. Moeller, and J. C. U. Zemella, Nat Photon **10**, 745 (2016).

[19] E. Allaria *et al.*, Nature Communications **4** (2013), 10.1038/ncomms3476.

[20] E. Ferrari *et al.*, Nature Communications **7**, 10343 (2016).

[21] J. Amman *et al.*, Nat. Photon. **6**, 693 (2012).

[22] A. A. Lutman, F.-J. Decker, J. Arthur, M. Chollet, Y. Feng, J. Hastings, Z. Huang, H. Lemke, H.-D. Nuhn, A. Marinelli, J. L. Turner, S. Wakatsuki, J. Welch, and D. Zhu, Phys. Rev. Lett. **113**, 254801 (2014).

[23] D. Ratner, R. Abela, J. Amann, C. Behrens, D. Bohler, G. Bouchard, C. Bostedt, M. Boyes, K. Chow, D. Cocco, F. J. Decker, Y. Ding, C. Eckman, P. Emma, D. Fairley, Y. Feng, C. Field, U. Flechsig, G. Gassner, J. Hastings, P. Heimann, Z. Huang, N. Kelez, J. Krzywinski, H. Loos, A. Lutman, A. Marinelli, G. Marcus, T. Maxwell, P. Montanez, S. Moeller, D. Morton, H. D. Nuhn, N. Rodes, W. Schlotter, S. Serkez, T. Stevens, J. Turner, D. Walz, J. Welch, and J. Wu, Phys. Rev. Lett. **114**, 054801 (2015).

[24] C. Emma, A. Lutman, M. W. Guetg, J. Krzywinski, A. Marinelli, J. Wu, and C. Pellegrini, Applied Physics Letters **110**, 154101 (2017), http://dx.doi.org/10.1063/1.4980092.

[25] E. Ferrari *et al.*, Scientific Reports **5** (2015), 10.1038/srep13531.

[26] A. A. Lutman *et al.*, Nat Photon **10**, 468 (2016), article.

[27] K. Prince *et al.*, Nat. Photon. **10**, 176 (2016).

[28] M. W. Guetg, A. A. Lutman, Y. Ding, T. J. Maxwell, F.-J. Decker, U. Bergmann, and Z. Huang, Phys. Rev. Lett. **120**, 014801 (2018).

[29] Y. Ding *et al.*, Phys. Rev. Accel. Beams **19**, 100703 (2016).

[30] S. Huang, Y. Ding, Y. Feng, E. Hemsing, Z. Huang, J. Krzywinski, A. A. Lutman, A. Marinelli, T. J. Maxwell, and D. Zhu, Phys. Rev. Lett. **119**, 154801 (2017).

[31] A. Marinelli, J. MacArthur, P. Emma, M. Guetg, C. Field, D. Kharakh, A. A. Lutman, Y. Ding, and Z. Huang, Applied Physics Letters **111**, 151101 (2017), https://doi.org/10.1063/1.4990716.

[32] M. Seibert *et al.*, Nature **470**, 73 (2011).

[33] A. Aquila *et al.*, Structural Dynamics **2**, 041701 (2015), https://doi.org/10.1063/1.4918726.

[34] A. Barty *et al.*, Nature Photonics **6**, 35 EP (2011).

[35] H. N. Chapman, C. Caleman, and N. Timneanu, Philosophical Transactions of the Royal Society of London B: Biological Sciences **369** (2014), 10.1098/rstb.2013.0313.

[36] L. Young *et al.*, Nature **466**, 56 (2010).

[37] J. Stöhr and A. Scherz, Phys. Rev. Lett. **115**, 107402 (2015).

[38] N. Rohringer *et al.*, Nature **481**, 488 (2012).

[39] C. Weninger, M. Purvis, D. Ryan, R. A. London, J. D. Bozek, C. Bostedt, A. Graf, G. Brown, J. J. Rocca, and N. Rohringer, Phys. Rev. Lett. **111**, 233902 (2013).

[40] N. Berrah *et al.*, Proceedings of the National Academy of Sciences **108**, 16912 (2011), http://www.pnas.org/content/108/41/16912.full.pdf.

[41] P. Emma, K. Bane, M. Cornacchia, Z. Huang, H. Schlarb, G. Stupakov, and D. Walz, Phys. Rev. Lett. **92**, 074801 (2004).

[42] C. Behrens *et al.*, Nature Communications **5**, 4762 (2014).

[43] Y. Ding, C. Behrens, R. Coffee, F.-J. Decker, P. Emma, C. Field, W. Helml, Z. Huang, P. Krejcik, J. Krzywinski, H. Loos, A. Lutman, A. Marinelli, T. J. Maxwell, and J. Turner, Applied Physics Letters **107**, 191104 (2015), http://dx.doi.org/10.1063/1.4935429.

[44] A. A. Zholents, Phys. Rev. ST Accel. Beams **8**, 040701 (2005).

[45] T. Tanaka, Phys. Rev. Lett. **110**, 084801 (2013).

[46] E. Prat and S. Reiche, Phys. Rev. Lett. **114**, 244801 (2015).

[47] E. Prat, F. Löhl, and S. Reiche, Phys. Rev. ST Accel. Beams **18**, 100701 (2015).

[48] C. Emma, K. Fang, J. Wu, and C. Pellegrini, Phys. Rev. Accel. Beams **19**, 020705 (2016).

[49] S. Huang, Y. Ding, Z. Huang, and G. Marcus, Phys. Rev. Accel. Beams **19**, 080702 (2016).

[50] J. MacArthur, J. Duris, Z. Huang, and A. Marinelli, in *8th Int. Particle Accelerator Conf.(IPAC'17), Copenhagen, Denmark, 14â 19 May, 2017* (JACOW, Geneva, Switzerland, 2017) pp. 2848–2850.

[51] A. Marinelli, R. Coffee, S. Vetter, P. Hering, G. N. West, S. Gilevich, A. A. Lutman, S. Li, T. Maxwell, J. Galayda, A. Fry, and Z. Huang, Phys. Rev. Lett. **116**, 254801 (2016).

[52] K. Bane and G. Stupakov, Nuclear Instruments and Methods in Physics Research Section A: Accelerators, Spectrometers, Detectors and Associated Equipment **690**, 106 (2012).

[53] E. Prat, S. Bettoni, and S. Reiche, Nuclear Instruments and Methods in Physics Research Section A: Accelerators, Spectrometers, Detectors and Associated Equipment **865**, 1 (2017), physics and Applications of High Brightness Beams 2016.

[54] Y.-C. Chao, SLAC-PUB-16935, SLAC (2018).

[55] W. Qin, Y. Ding, A. A. Lutman, and Y.-C. Chao, Phys. Rev. Accel. Beams **20**, 090701 (2017).

[56] Z. Zhang, K. Bane, Y. Ding, Z. Huang, R. Iverson, T. Maxwell, G. Stupakov, and L. Wang, Phys. Rev. ST Accel. Beams **18**, 010702 (2015).

[57] J. Zemella *et al.*, Phys. Rev. Accel. Beams **20**, 104403 (2017).

[58] S. Antipov, S. Baturin, C. Jing, M. Fedurin, A. Kanareykin, C. Swinson, P. Schoessow, W. Gai, and A. Zholents, Phys. Rev. Lett. **112**, 114801 (2014).

[59] P. Emma, M. Venturini, K. L. F. Bane, G. Stupakov, H.-S. Kang, M. S. Chae, J. Hong, C.-K. Min, H. Yang, T. Ha, W. W. Lee, C. D. Park, S. J. Park, and I. S. Ko, Phys. Rev. Lett. **112**, 034801 (2014).

[60] H. Deng, M. Zhang, C. Feng, T. Zhang, X. Wang, T. Lan, L. Feng, W. Zhang, X. Liu, H. Yao, L. Shen, B. Li, J. Zhang, X. Li, W. Fang, D. Wang, M.-e. Couprie, G. Lin, B. Liu, Q. Gu, D. Wang, and Z. Zhao, Phys. Rev. Lett. **113**, 254802 (2014).

[61] F. Fu *et al.*, Phys. Rev. Lett. **114**, 114801 (2015).

[62] G. Penco, E. Allaria, I. Cudin, S. Di Mitri, D. Gauthier, S. Spampinati, M. Trovó, L. Giannessi, E. Roussel, S. Bettoni, P. Craievich, and E. Ferrari, Phys. Rev. Lett. **119**, 184802 (2017).

[63] P. Heimann *et al.*, Review of Scientific Instruments **82**, 093104 (2011), https://doi.org/10.1063/1.3633947.

[64] J. J. Turner *et al.*, Journal of Synchrotron Radiation **22**, 621 (2015).

[65] S. Bettoni, P. Craievich, A. A. Lutman, and M. Pedrozzi, Phys. Rev. Accel. Beams **19**, 021304 (2016).

[66] P. Craievich and A. A. Lutman, Nuclear Instruments and Methods in Physics Research Section A: Accelerators, Spectrometers, Detectors and Associated Equipment **865**, 55 (2017), physics and Applications of High Brightness Beams 2016.

[67] N. Hartmann *et al.*, Nat. Photon. **12**, 215 (2018).

[68] S. Li, Z. Guo, R. N. Coffee, K. Hegazy, Z. Huang, A. Natan, T. Osipov, D. Ray, A. Marinelli, and J. P. Cryan, Opt. Express **26**, 4531 (2018).

[69] A. Sanchez-Gonzalez *et al.*, Nature Communications **8**, 15461 EP (2017), article.

[70] S. Bettoni, E. Prat, and S. Reiche, Phys. Rev. Accel. Beams **19**, 050702 (2016).